

## 6. Cooling

### 6.1 Introduction

The goal of this six-month study is an integrated design for a neutrino source, subject to realistic engineering constraints. As will become evident, the coupling between the cooling-channel design and the design of the upstream components is critical to achieving the best performance. Nevertheless, to make sufficiently rapid progress it has been necessary to design the various components semi-independently, then optimize and iterate to converge towards an integrated design. While we have not yet arrived at a fully optimized design, we have studied sufficiently the cooling channels described below to determine that their performance is limited primarily by the performance of the current phase-rotation and buncher designs. While the designs presented here suffice for an entry-level neutrino factory ( $10^{19}$  neutrinos /year) our overall conclusion is that further iteration of the integrated design is called for.

#### 6.1.1 Theory

The successful design of a high-intensity neutrino source requires that the transverse phase space occupied by the muon beam after the capture, phase-rotation, and buncher channels be reduced by a factor of  $\sim 10$  in each plane before it enters the acceleration section.

The technique which could accomplish this “beam-cooling” task within the time limit imposed by the finite lifetime of the muon is ionization cooling [1],[2],[3]. In ionization cooling, the beam, while passing through material, loses both transverse and longitudinal momentum by ionization energy loss ( $dE/dx$ ). The longitudinal momentum is then restored by passing the beam through accelerating cavities. This sequence results in a reduction of the angular spread of the beam particles and thus a reduction of the transverse emittance. However, multiple Coulomb scattering in the energy-absorbing medium heats the beam. To minimize this heating effect, the absorbers have to be placed in a strong focusing field. An approximate differential equation for the rate of change of the normalized transverse emittance  $\epsilon_n$  is

$$\frac{d\epsilon_n}{ds} = -\frac{1}{\beta^2} \frac{dE_\mu}{ds} \frac{\epsilon_n}{E_\mu} + \frac{1}{\beta^3} \frac{\beta_\perp (0.014)^2}{2E_\mu m_\mu L_R} ,$$

where  $s$  is the path-length,  $E_\mu$  is the beam energy,  $\beta = v/c$ ,  $L_R$  is the radiation length of the absorber medium, and  $\beta_\perp$  is the betatron function of the beam (the size of the beam is given by  $\sigma_z = \sqrt{\epsilon_n \beta_\perp / \beta \gamma}$ ). Since the heating term is proportional to  $\beta_\perp$  and inversely proportional to  $L_R$ , we need to place the absorbers in low- $\beta_\perp$  regions (strong focusing) and use material with high  $L_R$  (hydrogen) in order to maximize cooling. A detailed discussion of the principles of ionization cooling is presented in Refs [1] and [4].

To obtain the strong beam focusing needed for optimal cooling in the absorber, several lattice configurations have been considered. Focusing by solenoids has been selected based on the results of design studies, and on the engineering constraints imposed for a realistic cooling-channel design. Solenoidal focusing has the advantage of naturally focusing equally in both transverse planes, simplifying the design of the transverse beam optics. Solenoids could focus the beam to small  $\beta_\perp$  at absorbers in field-free regions, or could provide continuous focusing, with the absorbers placed inside the magnet, allowing the use of extended absorber lengths. The complication with the use of solenoids arises from the fact that a particle entering such a magnet acquires angular momentum, by its interaction with the radial component of the field at the entrance of the solenoid. In the absence of absorbers, this effect is reversible, since at the exit of the solenoid the particle receives an opposite kick from the radial field there, canceling the angular momentum acquired at the entrance. With an absorber within the solenoid, the beam loses angular momentum in the absorber, so at the exit the cancellation is not exact, and the beam retains a net angular momentum. If this angular momentum is not compensated, it results in emittance dilution. In the designs presented here, the technique used to compensate for this effect is to alternate the sign of the solenoidal field so that the sign of the residual angular momentum changes. In an ideal case, where this “field flip” is a step function, the solution would be to alternate the sign after every absorber, which implies variable focusing. Since the longitudinal and transverse motions are coupled, noticeable longitudinal emittance dilution can occur. As a result, the frequency with which we switch the sign of the field is one subject of optimization for each channel.

Each cooling channel is characterized by an optimum length. In the absence of longitudinal-transverse correlation, and at a fixed  $\beta_\perp$ -min, the transverse emittance settles to an equilibrium value, where additional cooling is compensated by re-heating due to multiple scattering. However, in practice, beyond that quasi-equilibrium point, the transverse emittance starts to increase with channel length, due to the continuous increase of the longitudinal emittance and this correlation.

Three sets of constraints on the design optimization of the cooling channels are imposed by 1) the beam coming from the upstream components of the front end, 2) the beam which the acceleration system that follows can accept, and 3) the engineering requirements for realistic component parameters. For instance, the cooling channel should not be configured independently of the buncher. This is because both the numbers and lengths of matching sections (longitudinal or transverse) must be minimized. In addition, with such large-emittance beams, matching sections are often difficult to design without beam losses. Hence, a significant part of the effort has been devoted to studying integrated solutions, in which a beam is propagated all the way from the pion production target to the beginning of the first accelerating linac.

### 6.1.2 Design Goals

An initial design study of all the components of a neutrino factory by Palmer, Johnson, and Keil (PJK) [5] concluded that the cooling needed is approximately one order of magnitude in each transverse plane. Our goal is to obtain this transverse cooling without unmanageable longitudinal dilution of the bunch. A factor  $\sim 1.4$  was to come from minicooling, thus the input emittance into the cooling channel was assumed to be  $\sim 10\pi$  mm.rad, and we targeted an output emittance of about  $1.5\pi$  mm.rad. The input rms bunch length was  $\sim 10$  cm and the momentum spread was  $\sim 10\%$ . The buncher was assumed to provide a beneficial longitudinal-transverse correlation (discussed in more detail below) since the bunching is done in a lattice similar to the ones used in the cooling channels.

While rms emittance provides a useful gauge of cooling performance, for a neutrino factory what counts most is the number of muons decaying in the straight sections of the storage ring. Thus the most directly useful measure of performance is the number of muons exiting the cooling channel within the acceptance of the acceleration system. This acceptance has been specified by the TJNAF group as a four-dimensional hypersphere in transverse phase space with radius equal to  $2.5\sigma$ , where  $\sigma^2 = 1.5\pi$  mm.rad, and an ellipse in longitudinal phase space with area of  $150\pi$  mm. Within these limits 99% of muons are expected to be accelerated and delivered to the storage ring, while a negligible fraction of muons lying outside of these limits will be accelerated. We regard the yield into this acceptance as our main figure of merit and will present it below for each cooling channel studied.

The buncher simulations available at present do not provide the beam just described, with consequent degradation of the performance of the cooling channels. The specifications of the input beams actually used in the cooling simulations are discussed in Sections 6.2.1 and 6.3.1.

### 6.1.3 Cooling Channel Lattices or Types

As of about a year and a half ago, our collaboration had studied basically one type of cooling channel, the Alternating Solenoid (AltSol) cooling channel. Since then, we have improved our understanding of this type of lattice, with analytical solution of the beam envelope equations in solenoidal channels [3][4][6] and detailed numerical simulations of AltSol at transverse emittances ranging from 12 cm down to 1.5 cm with linacs running at 175 MHz or 201 MHz. The LBL group has proposed a simpler sinusoidal-focusing-field configuration (FOFO). A biperiodic version of this lattice has also been studied, where the more pronounced  $\beta_{\perp}$ -min is at the absorber and the tamer one in the middle of the linac where a necessary cavity window sits. V. Balbekov and Ya. Derbenev propose a lattice featuring two constant solenoidal fields, running with opposite current such the total canonical angular momentum of the beam is preserved through cooling (Single-Flip). The FOFO channel is conceptually the most straightforward and has been simulated in great detail with two distinct codes (ICOOL [7] and DPGeant[8]). This is our baseline, or reference design. The optimization – currently in progress – of this FOFO channel is tightly coupled to the performance of the upstream components of the front-end complex and engineering constraints. Since the performance of a realistic design (all constraints applied) could be worse than expected from the initial design, we have chosen to study (first with a less-detailed standalone Monte Carlo program, then with DPGeant) a second channel as a backup. This channel uses the single-flip lattice, chosen primarily because of the simplicity of its design. At this stage, both configurations have been reviewed from an engineering standpoint (more extensively in the FOFO case), and both succeed in cooling transversely without unacceptable dilution of the longitudinal phase space.

## 6.2 The Baseline FOFO Channel

### 6.2.1 The Input Beam

The design of the FOFO cooling channel was initially optimized using an idealized beam, since the design of the components of the machine upstream of the cooling channel was not completed at the time. The parameters of this idealized beam are given in Table 1. The final (“integrated-front-end”) optimization, currently in progress, uses the

beam at the exit of the buncher. It is important to note that the integrated-front-end design (including the induction linac and the buncher) used for the FOFO simulation differs from the baseline design presented in the preceding chapter and is based on an earlier design of the phase-rotation channel.

PARAMETER	VALUE
<b>Global</b>	-
Length of a section (1/2 of a lattice period)	1.1 m
Maximum magnetic field on axis	3.4 T
Number of sections	150
$\beta_{\perp}$ -min	35 cm
$\beta_{\perp}$ -max	88 cm
<b>Absorber</b>	-
Length of liquid-hydrogen (LH2) absorber	12.6 $\rightarrow$ 13.2 cm
Density of LH2	0.0708 g/cm <sup>3</sup>
Absorber window thickness	400 $\rightarrow$ 200 $\mu$ m
Absorber window material	Aluminum (6061-T6)
Energy loss per section, nominal	4.0 MeV
Radial aperture, in LH2	15.0 $\rightarrow$ 10.0 cm
<b>Linac</b>	-
Length of linac (per section)	66 cm ( $\pi/2$ ) or 74.56 cm ( $\pi$ )
Number of rf cells	2 ( $\pi/2$ ) or 1 ( $\pi$ )
Frequency	201.25 MHz
Peak electric field, on axis	15 MV/m ( $\pi/2$ ) or 18 MV/m ( $\pi$ )
Optimum synchronous phase ( $\phi_s$ )	$\sim$ 30 degrees
Acceleration at $\phi_s$	$\sim$ 4.0 MeV
Beryllium-window thickness (pillbox)	125 $\mu$ m
Radial aperture, linac	17 cm
<b>Beam</b>	-
Nominal momentum $p_0$	200 MeV/c
Normalized transverse emittance $\epsilon_n$	$\sim$ 15 $\pi$ mm rad
$\sigma(p_x)$	$\sim$ 25 MeV/c
Longitudinal bunch spread $\sigma_z$	$\sim$ 310 ps = 8.14 cm
Normalized longitudinal emittance $\epsilon_{Ln}$	$\sim$ 35 $\pi$ mm
Average momentum	$\sim$ 200 MeV/c
Momentum spread	$\sim$ 7 to 10 %
Longitudinal-transverse correlation	0

**Table 1:** Parameters of the FOFO cooling channel. The idealized input-beam parameters are given, although simulations have also been done with the beam coming out of the buncher, which has slightly different parameters and correlations.

As in the baseline design, in the integrated-front-end simulation, the cooling-channel input beam has been bunched at 201.25 MHz rf frequency, but it is matched to a beta function of  $\sim$ 35 cm at the null of the magnetic field. The central momentum is 200 MeV/c and the rms energy spread is 17 MeV (momentum spread of 20 MeV/c). The normalized rms transverse emittance is 9.1 $\pi$  mm.rad and the longitudinal emittance is 58  $\pi$  mm. There is negligible canonical angular momentum in the beam. The longitudinal phase space occupied by the particles spreads out beyond the separatrix of the rf bucket. There are 0.07 muons per proton overall, a factor 3 fewer than in the baseline design, and 0.05 muons per proton within a longitudinal phase-space area of 150  $\pi$  mm, which is the acceptance of the acceleration section. There is negligible correlation between the transverse amplitude and energy. This implies an additional mismatch into the rf system, as the FOFO channel is tuned for an energy-amplitude correlation  $\langle \Delta E \rangle / \langle A_{\perp} \rangle = 0.5$  GeV/m.

## 6.2.2 Technical Description

The lattice is periodic, characterized by a solenoidal magnetic field whose magnitude on axis varies sinusoidally with 2.2-m period and 3.4-T amplitude (Figure 3). The betatron phase advance per magnetic period is quite large by normal standards. This allows a relatively low  $\beta_{\perp\text{-min}}$  to be achieved with reasonable values for the on-axis field. However, the betatron resonance characteristic of such a simple and compact optical system leads to beam instabilities: as particles undergo synchrotron motion, their momentum can get close to the resonant momentum, leading to dramatic increase of the radial excursions. Unless favorable multiple scattering or straggling occurs, such particles are lost. The cooling process *de facto* weakens the impact of such betatron resonances.

Engineering feasibility is a complicated function that depends on such parameters as field, current density, and stress on the conductor. While a detailed engineering study has yet to be performed, a conservative rule of thumb (based on keeping the hoop stress within manageable limits) for solenoids built from Nb<sub>3</sub>Sn superconductor is [9]  $BJR < 350$  MPa, where  $B$  is the field at the coil,  $J$  the area current density, and  $R$  the radius, all evaluated at the location within the coils where the above product is at a maximum. Coils satisfying this inequality should have forces on the windings that are within acceptable engineering limits. The maximum magnetic field occurs on the facing surfaces of the “bucked” coil packs (see Figure 1), and this is also where the force on the windings will be greatest. For the 3.4-T FOFO the relevant values are  $B = 7.0$  T,  $J = 49$  A/mm<sup>2</sup>,  $R = 0.9$  m, giving  $BJR = 310$  MPa.

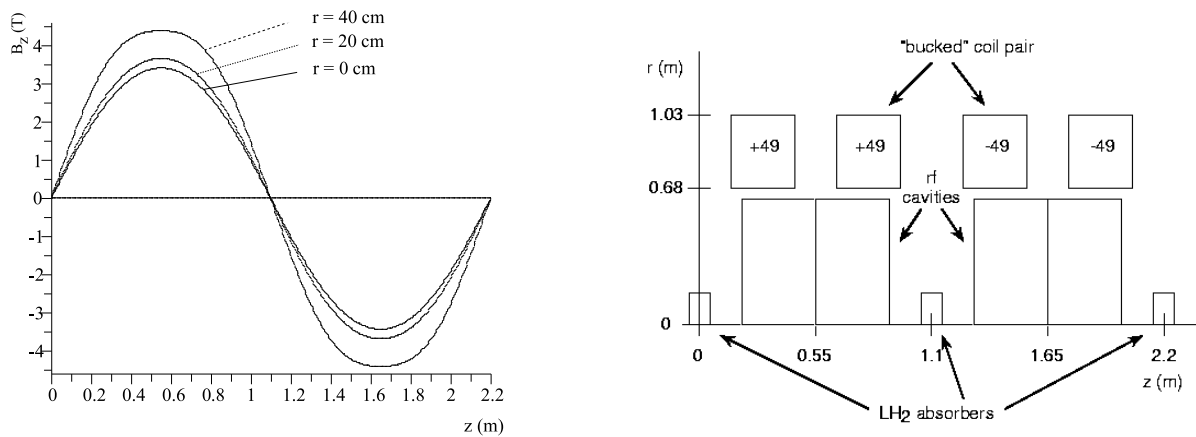


**Figure 3:** The profile of the longitudinal component of the magnetic field in the FOFO channel on axis and at 20- and 40-cm radius.

**Figure 1:** Sketch of a FOFO lattice period showing the relative locations of the coils, linac and absorbers. The LH<sub>2</sub> vessel and the linac are centered on the symmetry points of the section, at  $z = 0$  and  $0.55$  m, respectively.

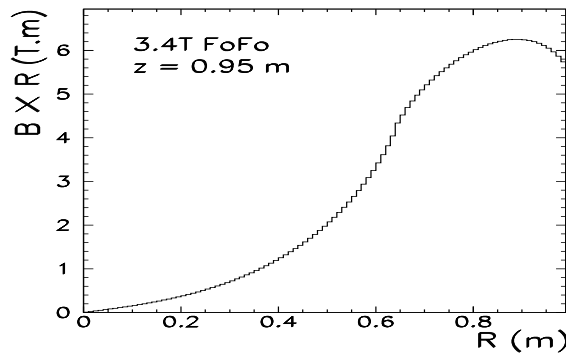


**Figure 2:** The magnetic field times the radius on the inner faces of the “bucked” coils (one of the critical factors entering into the design of such solenoids) vs. radius.

(see Figure 2). While the forgoing cannot substitute for a full engineering study, comparisons with existing magnets of similar size, function, and field production suggest that such current density can be reliably achieved in these magnets. The absorbers and linac structure are inserted into the lattice as shown in the engineering drawing of

Figure 4. Liquid-hydrogen (LH<sub>2</sub>) absorbers are used to minimize multiple scattering. The specifications of the absorbers are given in Table 1.

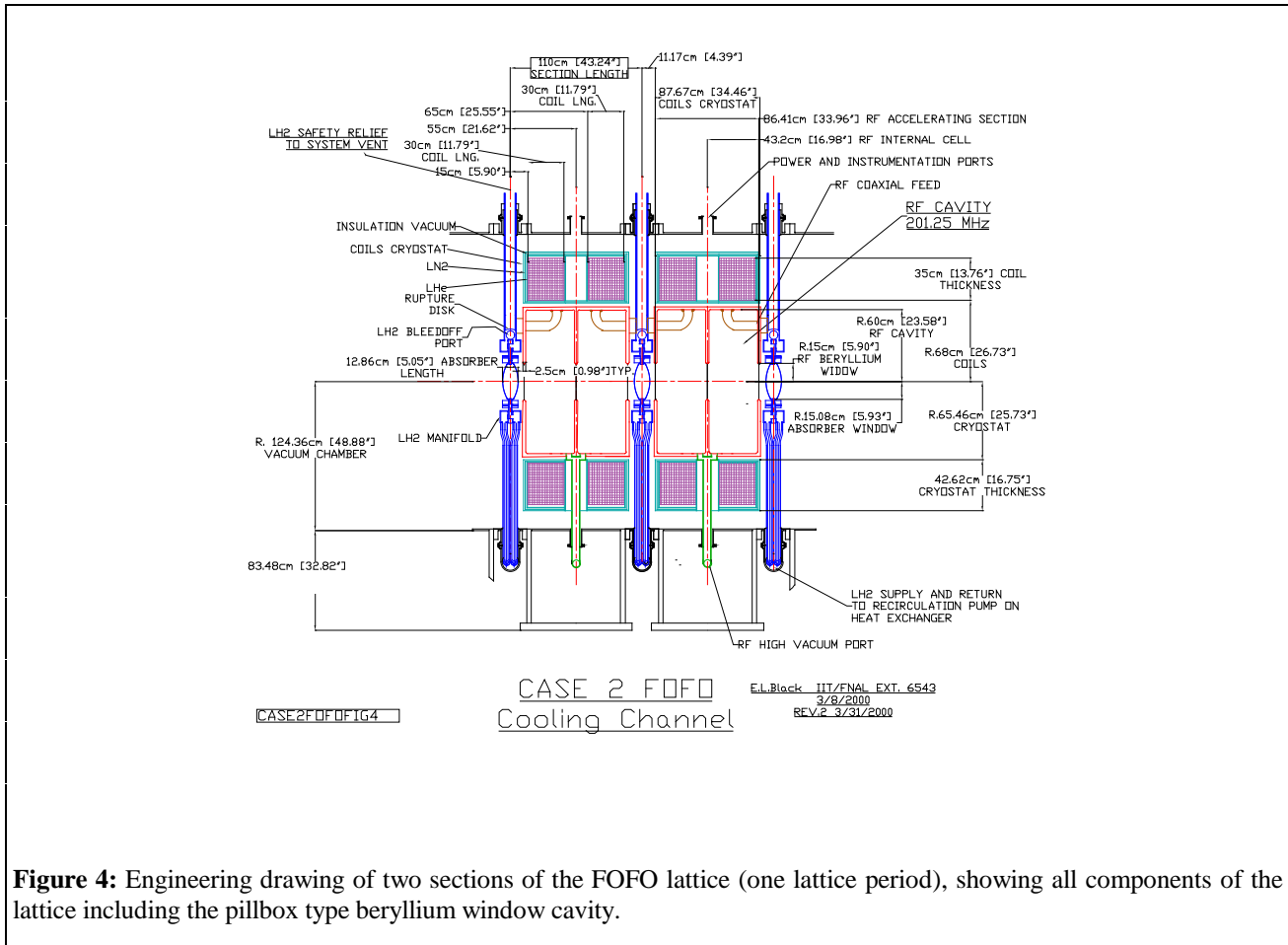


**Figure 4:** Engineering drawing of two sections of the FOFO lattice (one lattice period), showing all components of the lattice including the pillbox type beryllium window cavity.

The thickness of the absorber windows is a critical parameter. They must be thick enough to sustain the pressure from the LH<sub>2</sub> yet as thin as possible to reduce multiple scattering. The window thicknesses have been chosen based on the ASME standard for pressure vessels [10]. This choice also satisfies the Fermilab safety code for liquid-hydrogen targets [11]. Given the oblate shape of the absorbers, of three standard window profiles specified by ASME (hemispherical, ellipsoidal, and torispherical), the torispherical profile is chosen in order to minimize the sagitta and leave sufficient room for absorber connections and support structure (see Figure 6Figure 5). For this case, the minimum window thickness is given by

$$t = 4 \frac{0.885PD}{SE},$$

where  $P$  is the pressure differential,  $D$  the absorber diameter,  $S$  the ultimate strength of the window material, and  $E$  the weld efficiency. (This formula includes the safety factor of 4 mandated by ASME.) We have used  $S = 289$  MPa as given by ASME for 6061-T6 aluminum alloy and  $E = 0.9$ . We assume operation of the absorbers at an internal pressure of 1 atm, giving a 1-atm pressure differential on the windows.

Assuming that aluminum-alloy windows are used, the LH<sub>2</sub> and absorber windows in each cell correspond respectively to 1.45% and 0.90% of a radiation length in the first part of the channel, and 1.52% and 0.45% in the second. The reduction in window thickness from part 1 to part 2 of the channel is made possible by the reduction in transverse size of the beam and a corresponding reduction in the diameter of the absorber. It results in a lowering of the equilibrium emittance from  $2.6\pi$  mm.rad to  $2.2\pi$  mm.rad and a corresponding increase in the cooling rate. While

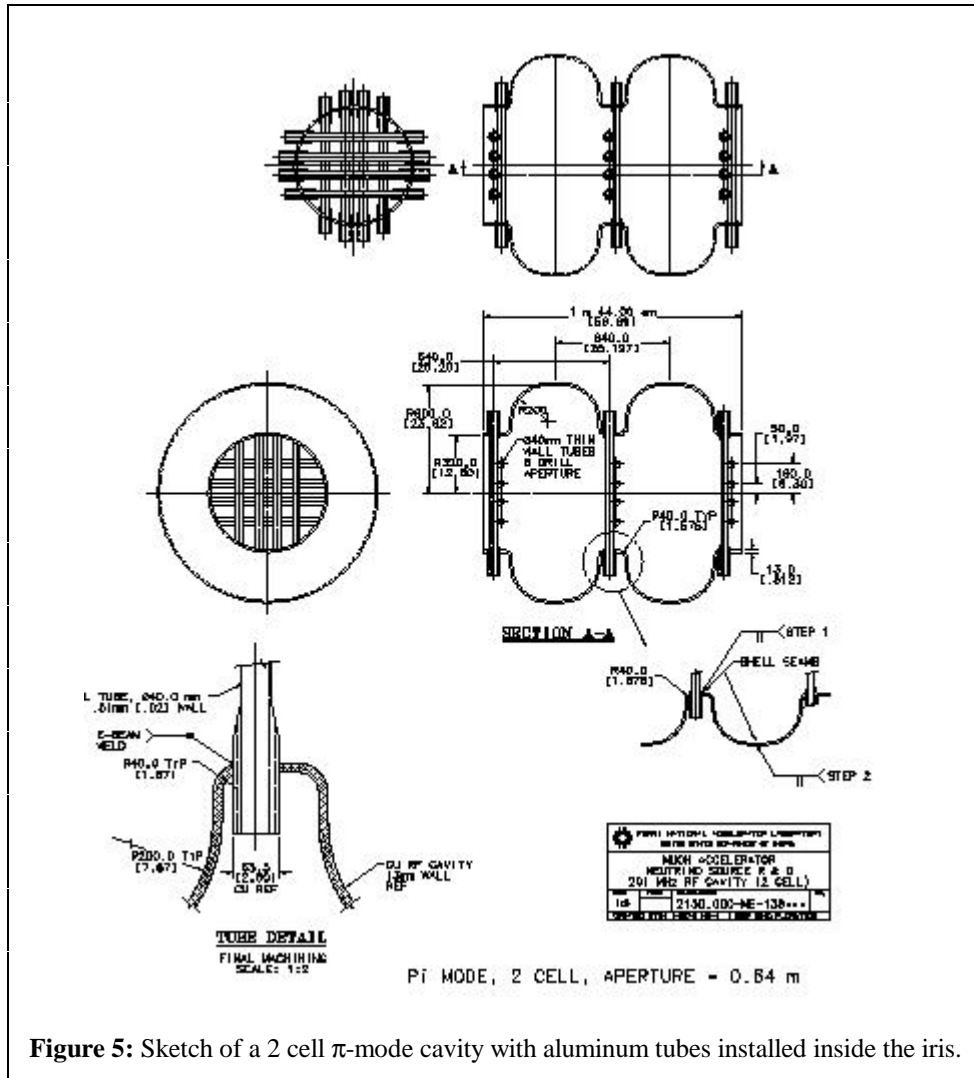
beryllium or AlBeMet (a composite of 62% beryllium/38% aluminum) could reduce the impact of the windows on the cooling performance, based on the CEA bubble-chamber accident, beryllium is believed to be incompatible with liquid hydrogen, and an R&D program would be required to establish safe design parameters for these materials.

In passing through the absorber, a 200-MeV/c muon loses on average 4 MeV of energy. Thus at the beginning of the channel, where bunches of up to  $10^{13}$  muons may be incident at a 15-Hz repetition rate, up to 100 W of power will be dissipated in each absorber. While larger than the power dissipations at which hydrogen targets have been operated at Fermilab, this is within the range of dissipation that has been handled successfully at SLAC [12] and Bates [13], utilizing a flow-through cooling-loop design with external heat exchanger. Engineering studies are ongoing to certify the power-handling performance of the absorber design which will be tested in a high-intensity beam as part of the R&D program for a neutrino factory or muon collider.

### 6.2.3 The Normal Conducting Accelerating Structure for the Cooling Channel

The linac has two functions: it provides the longitudinal focusing and compensates for the energy loss in the absorber. These linacs must be relatively compact in order to minimize the decay loss, hence relatively high accelerating gradient must be used. The number of cells per linac (or section) is driven by the period of the lattice, the resonating mode, the frequency and the momentum. These last two parameters are dictated by the bunch properties coming out of the buncher. The most straightforward option is to use the same frequency, 201.25 MHz.

The accelerating field provided by the rf systems in the cooling channel requires substantial rf power. Using closed-end accelerating cell structures, which allow arbitrary phase variation from cell-to-cell, allows the shunt impedance of multi-cell cavities to be increased significantly over open-cell structures, hence reducing rf power requirements. The



challenges in cell design and in rf power sources remain key technological areas. While the rf power sources are discussed in more detail in chapter 10, the cavities are an integral part of the cooling system.

There are two types of cavities under consideration for the ionization cooling channel. One is a pillbox cavity with thin beryllium windows covering the iris. The other is a cylindrical rf cavity with rounded ends and thin walled hollow aluminum tubes covering the beam aperture. Both cavities fit in the proposed cooling channel and have an outside radius, including copper wall thickness, of  $\leq 0.60$  m. The number of cells in the cooling channel is determined by the total ionization loss and the rf phase at which the muon bunch is accelerated.

The design with beryllium windows (pillbox type) has a 10 to 15 % larger optimized shunt impedance. This is important because the larger shunt impedance would require less rf power installed. A second advantage of the beryllium cavity design is that it achieves high accelerating gradients without increasing the peak surface electric field. However, because the beryllium needs to be thin, 125 microns, to reduce beam scattering, mechanical strength and thermal stability due to surface current heating are of major concern. The thin walled aluminum tube design, on the other hand, may be easily cooled by forced air or helium gas flow through the tubes. The tubes are mechanically more stable and less prone to rupture than are the beryllium windows. The diameter of the tubes is 4 cm and the walls range in thickness from  $\sim 100$   $\mu\text{m}$  at the beam center up to 150  $\mu\text{m}$ . A sketch of a  $\pi$ -mode cavity with tubes inside the iris is shown in Figure 5. The thin beryllium windows of large radius can only support a small pressure differential. In addition the aluminum tube design is expected to be less expensive. Its mechanical strength can be designed to operate with beam apertures as large as 0.64m. This may be important in the early stages of the cooling channel where the muon beam is the largest. There are currently draft mechanical designs for both cavity designs (one example is shown in

Figure 4). The thin walled aluminum tube design comes at the expense of a higher peak surface electric field gradient. At the surface of the tubes, the surface electric field is increased by a factor 1.5 relative to the accelerating gradient. This could limit the peak achievable accelerating gradient due to vacuum electrical breakdown in the cavity, and perhaps multipacting.

Both designs should achieve the design gradient of 15 MV/m. In fact experiments performed on the Fermilab 200 MHz linac have achieved gradients of 40 MV/m in pulsed operation. Using closed-end structures (with Be window or Al tubes), allow the shunt impedance

of multi-cell cavities to be increased over open-cell structures, hence reducing rf power requirements. The beryllium design requires an rf power of 5.6 MW for an accelerating gradient of 15 MV/m. The aluminum tube design requires an rf power of 6.2 MW and has a peak surface electric field of 22.5 MV/m. The peak power production and distribution is discussed in more detail in chapter 10. An example is given in Table 2. While the pillbox has a relatively short transit time, the muons always go through three windows per linac structure. Detailed simulations based on 3D particle tracing are needed to estimate the beam dynamics and the scattering probability in the grid or window. This effort is ongoing.

Parameter	Crossed Tube	Pill Box
Frequency	201.25 MHz	201.25 MHz
Accelerating Phase Angle	Sin(25 degrees)	
Peak Accelerating Field	15.0 MV/m	15 MV/m
Peak Surface Field	22.5 MV/m	15 MV/m
Kilpatrick Limit	14.8 MV/m	14.8 MV/m
Cavity Type	Open Cell with crossed tubes over aperture	Beryllium foil windows over 15 cm radius apertures
Cavity Dimensions	internal r is 0.600 m internal cell length, $\lambda\beta/3$ , is 0.432 m.	internal radius is 0.600 m, internal cell length, $\lambda\beta/3$ , is 0.432 m. length of accelerating section is 0.864 m.
Impedance	28.4 M $\Omega$ /m	34.1 M $\Omega$ /m
Shunt Impedance	20.3 M $\Omega$ /m	23.3
Transit Time Factor T	0.845	0.827
Peak Voltage per Cell	6.5 MV	5.7 MV
Q	47,500	52,600
Fill Time	38 $\mu\text{s}$ , critically coupled	42 $\mu\text{s}$
rf Pulse	114 $\mu\text{s}$	125 $\mu\text{s}$
Peak Power per Cell	3.45 MW	2.8 MW
Average Power per Cell	8.0 kW	5.3 kW
Window Type	4 cm diameter Al crossed tubes	15 cm radius, 127 $\mu\text{m}$ thick Be foil
Average Power on Tubes	30 W (worst tube)	53 W (heated from both sides)

**Table 2:** Example rf cavity parameters for a 1.1 m channel with an aperture of 34 cm and  $2\pi/3$  phase advance per cell.

We take the Pillbox type, running in the TM010 mode, with  $\pi/2$  phase advance per cell, equipped with thin beryllium windows, with two cells per linac as the baseline for this study. For cooling simulations it is interesting to note, that while the first cavity has a relatively short transit time, the muons always go through three windows per linac structure. Detailed simulations based on 3D particle tracing are needed to estimate the beam dynamics and the scattering probability in the grid or window. This effort is ongoing. We take the pillbox-type cavity as the baseline for this study.

### 6.2.4 Performance

As mentioned above, the cooling channel cannot be designed in isolation but must be optimized together with the muon source “front-end” components that precede it. This work has not yet been completed to our satisfaction, and what we present here is in the nature of a status report. Prior to availability of a simulated output beam from the buncher and matching section, we explored the optimization of the FOFO channel using an approximation of the expected beam that would be input to it, and Figure 7 summarizes the resulting cooling performance for this idealized beam. The parameters of the channel are similar to those described above. Muon decay losses have been turned off in the simulation in order to isolate optics and matching issues but contribute an additional 12% loss.

The large (50%) losses in the first 25 m of the channel reflect the need for further optimization, and in particular the need to incorporate a realistic longitudinal-transverse correlation in the incoming beam, such as would be present in the beam from the buncher but is absent in this simulation. The desired correlation ameliorates the differential path length through the lattice for muons at large transverse amplitude (which follow helical trajectories with large radii) compared to those at small transverse amplitude (whose helices have small radii) by raising the average muon energy in proportion to transverse amplitude. Despite the absence of such correlation, Figure 7b shows that the transverse emittance is cooled by a factor of 7 over the 150 m of the cooling channel, approaching the PJK goal [5].

Figure 7c shows the number of muons within the acceptance of the acceleration system (see Section 6.1.2), which is seen to increase by a factor 4.5 within the first 120 m of the channel and then to decline with continued longitudinal phase-space dilution and beam losses. Better performance is expected once the losses at the beginning of the channel have been optimized.

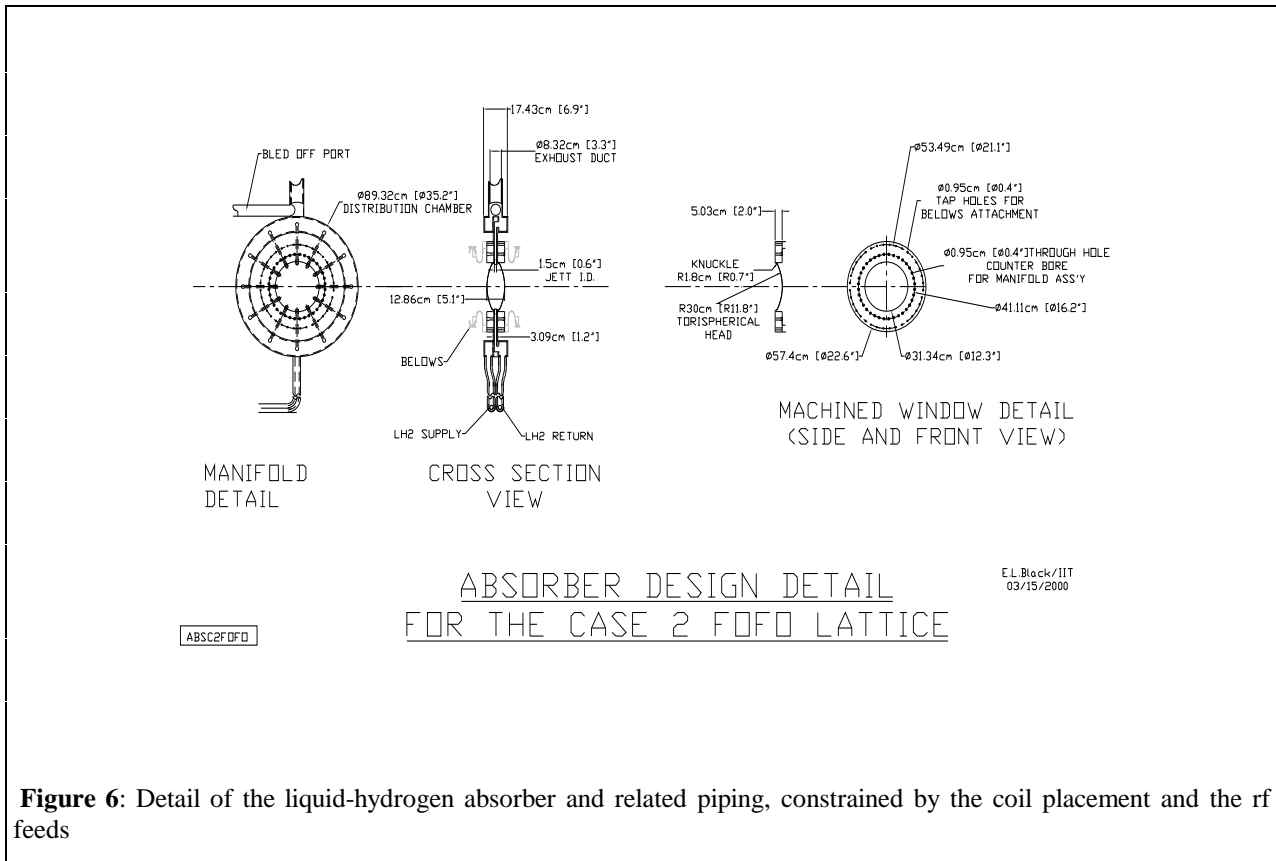


**Figure 6:** Detail of the liquid-hydrogen absorber and related piping, constrained by the coil placement and the rf feeds

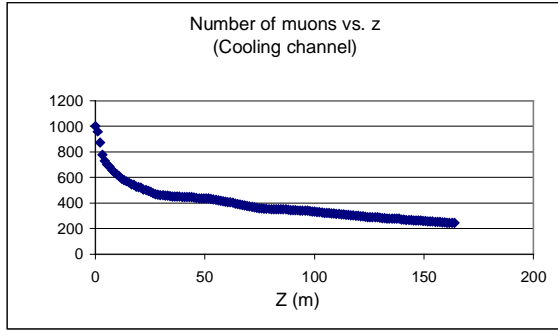


**Figure 7a:** Transmission in the FOFO channel vs. distance using the idealized beam described in the text.

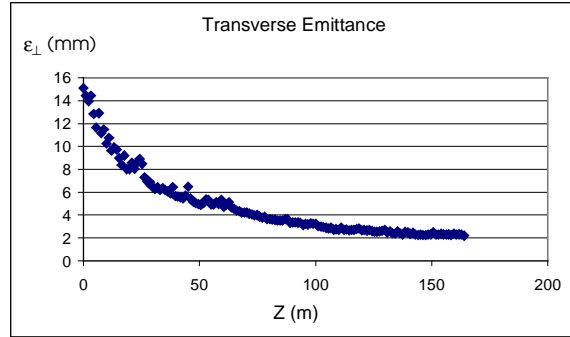


**Figure 7b:** Transverse emittance vs. distance for the idealized beam.

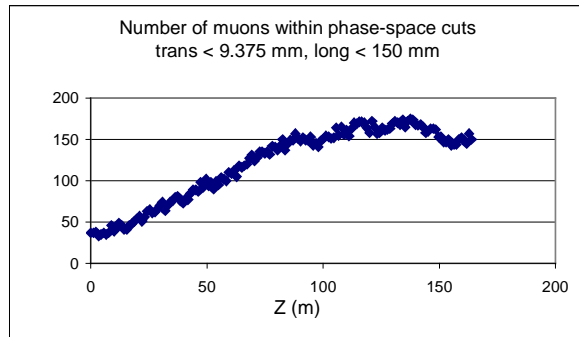


**Figure 7c:** Relative yield increase within the acceptance of the accelerator ( $9.375\pi$  mm.rad transverse,  $150\pi$  mm longitudinal) using the idealized beam.

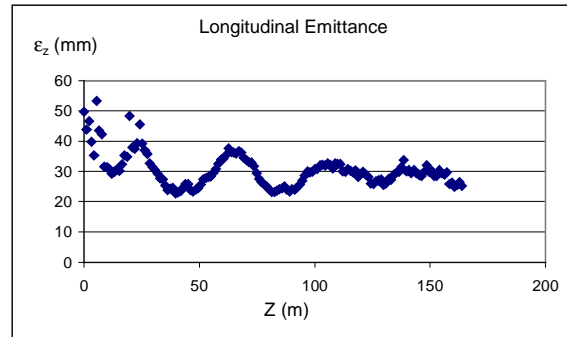


**Figure 7d:** The longitudinal emittance of the idealized beam in the FOFO channel.

**Figure 7:** Summary of cooling performance of the channel with an idealized beam.

We next present results from the integrated-front-end simulation. The parameters of the channel have been given above. Figure 8 summarizes its performance. While the final transverse emittance obtained is similar to that with the idealized beam, the cooling factor is smaller since the beam begins with a smaller emittance ( $9.2\pi$  mm rad). The losses are also worse, with the total yield into the acceleration system increasing by a factor of only 2 within the first 100 m of the channel, to 0.018 muons/proton. While the number of muons within the acceleration acceptance declines in the last 50 m, we have left the length of the cooling channel at 150 m in the cost estimate, both to be conservative and to leave room for possible additional beam manipulations.

Insight into the large losses and poor performance of these simulations so far is provided by Figure 9, which shows the longitudinal phase plane at the input of the cooling channel and 65 m further downstream. The input beam has a time spread that extends well beyond the separatrix, thus the large initial losses are not surprising. The continued losses along the entire length of the channel reflect the behavior expected when an overfull bunch is presented at the input, since the longitudinal emittance dilution due to stochastic effects in the absorber necessarily causes particles near the separatrix to cross into the unstable region of the phase plane.

This performance represents a notable shortfall relative to the PJK design sketch [5], but we are confident that there is substantial room for improvement with further optimization work and R&D. As an example, we have simulated a FOFO channel with parameters similar to those described above except that the absorber windows have been eliminated. While liquid-hydrogen absorbers do require containment, this case indicates how much might be gained by R&D on exotic window materials such as beryllium or AlBeMet. The yield within the acceleration acceptance is increased by 50%. Moreover, the FOFO lattice may not be the optimal choice for muon cooling in this emittance range, an issue that will be elucidated by further work on the single-flip and alternating-solenoid options.

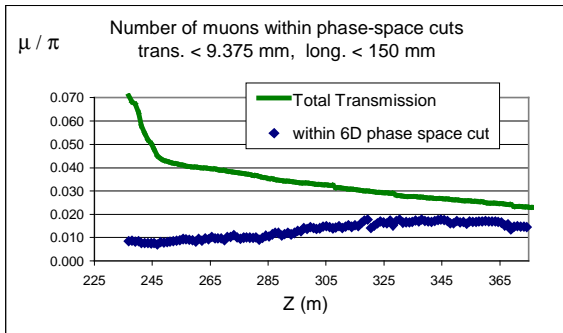


**Figure 8a:** The transmission vs. distance and the muon yield within the acceptance of the accelerator.

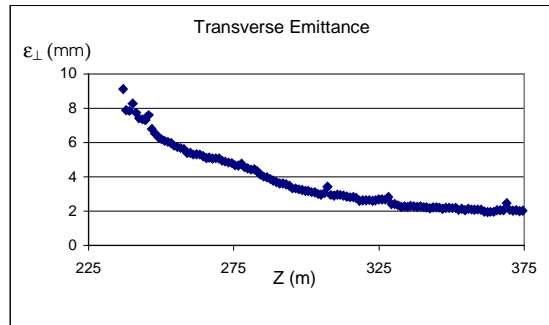


**Figure 8b:** The transverse emittance vs. distance in the FOFO cooling channel.

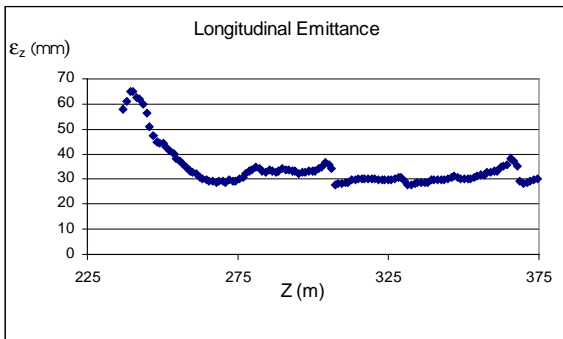


**Figure 8c:** The longitudinal emittance.

**Figure 8:** Summary of the integrated-front-end simulation.

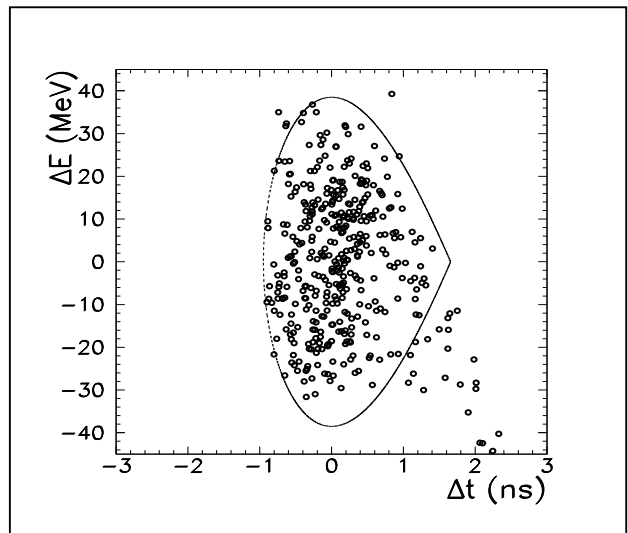
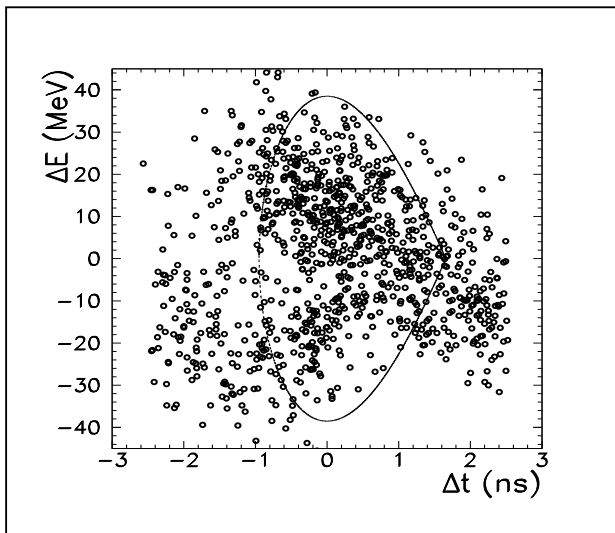


**Figure 9:** The longitudinal phase space of the bunch entering the FOFO cooling channel (left) and 65m further downstream (right). Muons from the integrated simulation are shown together with an approximate representation of the separatrix.

### 6.3 The Single-Flip-Channel Option

Unlike the baseline FOFO channel, this channel has a very simple lattice (Figure 10): the cooling sections use continuous focusing from long solenoids, with the absorbers placed inside the magnets. Such a configuration provides simple transverse optics: for a matched beam there is no modulation of the beam envelope in the channel. The field of the long solenoid is reversed in the middle of the lattice, in order to control angular-momentum growth (see section 6.1.1). A special matching section is used at this point, both to minimize the length of the region affected by the polarity change, and to mitigate particle loss due to the excitation of synchrotron oscillations. These oscillations arise from the longitudinal-transverse phase-space correlations that develop due to the dependence of the time of flight on the transverse amplitude of the particles in a solenoid. The transverse momentum and thus the transverse amplitude changes at the field reversal; this change has to occur in a spatial region smaller than the Larmor wavelength of the beam in order to control these effects.

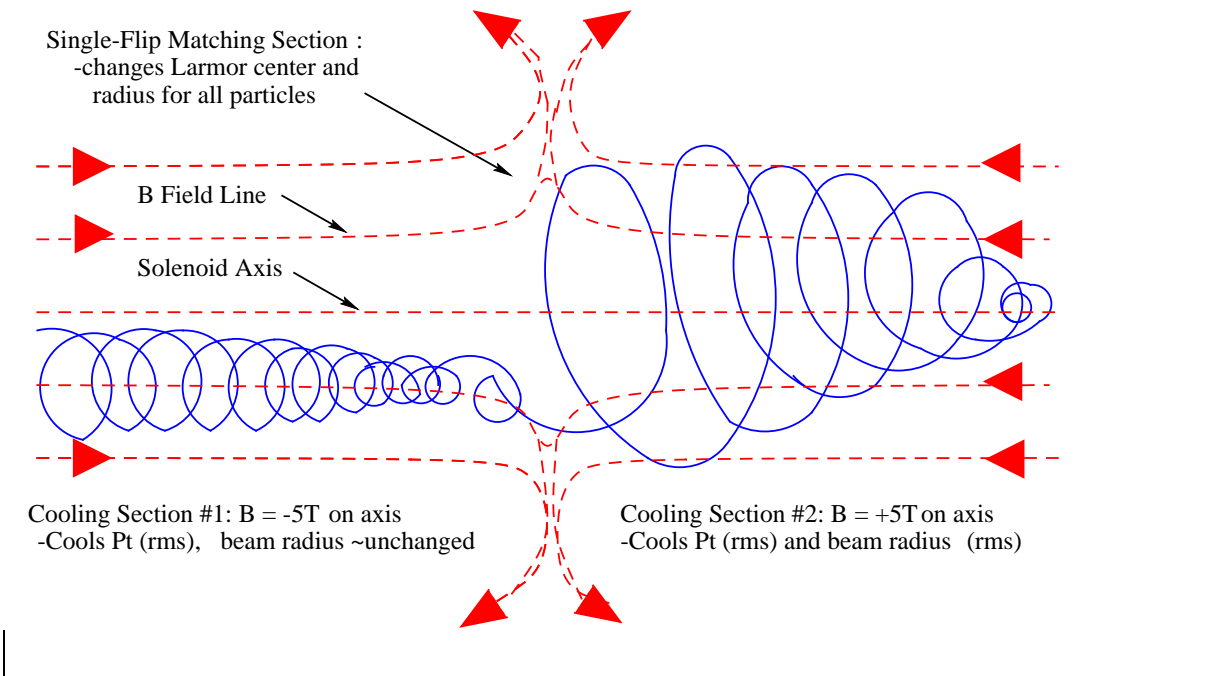
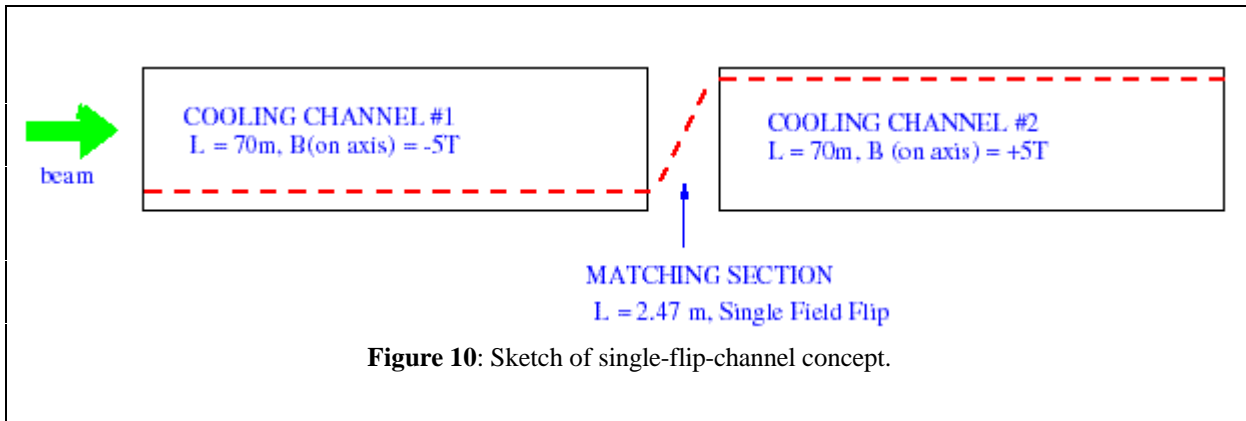


Figure 11 illustrates the cooling principle of the single-flip channel. Channel 1 cools the transverse momenta of the muons, to first order without affecting the transverse size of the beam (to second order the beam grows slightly due to multiple scattering). (For an infinitely long channel, neglecting scattering, the muon helices would shrink to lines.) In the matching section between channels 1 and 2, the centers of the Larmor orbits are displaced such that in channel 2 the muons to first order execute Larmor motion about the solenoid axis. As this motion cools, both the beam size and transverse momenta are reduced.

### 6.3.1 Initial constraints and the input beam

The design of this channel is optimized to maximize the transmission and the cooling performance for the exact input beam produced at the end of the buncher described in the preceding chapter. As noted above, the optimization of any cooling channel is strongly coupled to the front-end design. The beam is relatively large:  $\sigma_x = 4.5$  cm,  $\sigma_{px} = 30$  MeV/c,  $\sigma_E = 40$  MeV, but it is the result of our initial global optimization given the constraints of all subsystems.

### 6.3.2 Technical description of the channel

This cooling lattice consists of two supersections: the first contains 28 cooling sections, 2.47m long, in an almost-constant magnetic field of  $-5T$  on axis. Between the two supersections there is one 2.47-m-long matching section in which the field changes polarity. The field flip is followed by a second supersection of 28 sections, 2.47-m long, at  $+5T$  on axis. Within each supersection the magnetic field varies as little as possible. A perfectly constant field would be ideal, however this cannot be achieved due to engineering constraints. Gaps in the solenoids required for rf power feeds and absorber cooling equipment are included in the simulation (see Figure 12).

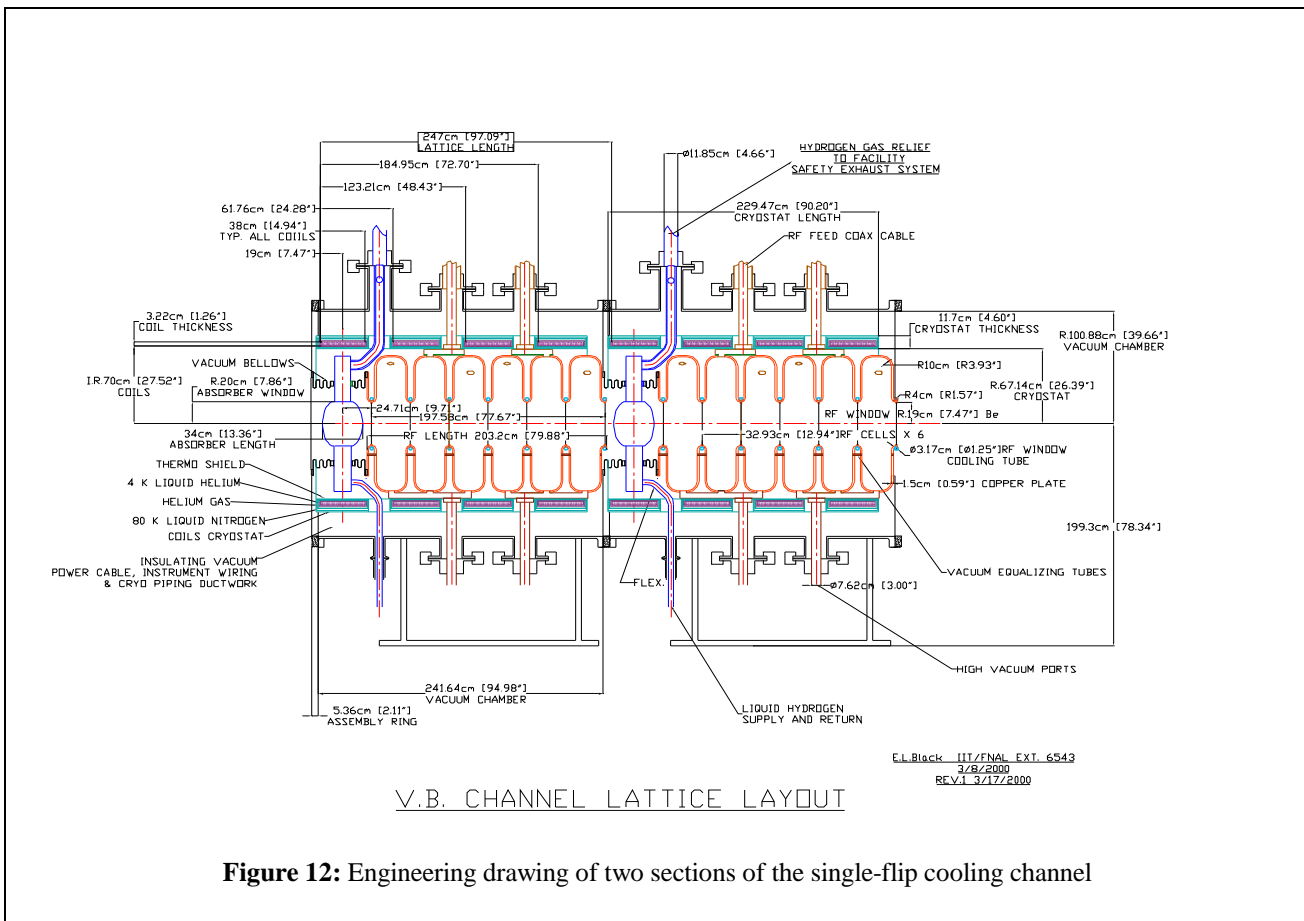


Figure 12: Engineering drawing of two sections of the single-flip cooling channel

The specifications of the cooling sections are given in Table 3. Each cooling section contains one liquid-hydrogen absorber and one linac consisting of  $6\pi/2$  TM010-mode pillbox cavities. The absorbers are wider in diameter than they are long, but they are longer than in the FOFO case, allowing use of the ellipsoidal window profile and a concomitant decrease in window thickness. For ellipsoidal windows, the minimum thickness is given by [10]

$$t = 4 \frac{0.5PD}{SE},$$

giving  $t = 300 \mu\text{m}$  as shown in the table. Note that the preliminary design for the cooling solenoids specifies 3-cm-thick coils at a current density of  $400 \text{ A/mm}^2$ . While this current density is within the specifications of NbTi superconductor for fields below 7 T [14], it implies a hoop stress  $BJR = 1800 \text{ MPa}$ , exceeding the conservative limit used for the FOFO coil design (see Section 6.2.2). If hoop stresses need to be reduced, thicker coils at reduced current density could easily be used.

An absorber of length 32 cm will scatter the beam with an rms angle of approximately 0.016 rad. The initial rms angular spread of the beam is 0.160 rad. At the end of the first supersection, the rms angular divergence of the beam is 0.048, still larger than the multiple-scattering contribution. The length of this supersection could be extended to reach the multiple-scattering limit. However, the length is chosen both to minimize the length of the cooling channel and to compensate for the expansion of the beam envelope in the matching section. The length of the second supersection is additionally constrained by the requirement that the beam be canonical after the cooling channel. By design, the nominal particle gains 12.5 MeV per linac and loses 10 MeV per absorber, thus the nominal channel momentum increases linearly by 2.5 MeV per 2.47-m-long section. This acceleration is chosen to increase the size of the rf bucket and compensate for the increase of the rms energy spread through the channel. In 28 sections, the rms momentum increases from 30 to 36 MeV/c due to the range of path lengths in the absorbers. The goal of increasing the bucket size is to avoid particle loss due to this longitudinal phase-space dilution.

Given the momentum dependence of ionization energy loss, to lose 10 MeV per absorber, the absorber lengths must increase with longitudinal position as the beam momentum increases. In the first supersection, absorber lengths increase from 31.6 cm in the first cell to 33.8 cm in the 28th cell. The absorber length is constant at 34 cm in the second supersection. The beam starts out at a momentum of about 200 MeV/c, enters the matching section around 280 MeV/c, and exits the second supersection at 340 MeV/c.

The most sensitive parameter of the cooling channel is the gradient of the magnetic field in the field-flip region. This gradient must be maximized in order to stabilize the longitudinal motion. This is achieved by inserting two sets of coils, at differing radii, in the region of the field flip. The

PARAMETER	VALUE
<b>Global</b>	-
Length of a section, $\Delta L$	2.47 m
Magnetic field on axis	5.0 Tesla
Magnetic field at the coil	6.3 Tesla
Field variation	0.02%
Current density	4,000,000 A/m
Coil radius	70 cm
$\beta_{\perp \text{ min}} (z = 0)$	21 cm
Number of sections per supersection	28
<b>Absorber</b>	-
Length of hydrogen (LH2) absorber	31 $\rightarrow$ 34 cm
Density of LH2	0.0708 g/cm <sup>3</sup>
Thickness of absorber windows	300 $\mu\text{m}$
Material for absorber windows	Aluminum
Energy loss per section, nominal	$\sim$ 10 MeV
Radial aperture, in LH2	$r = 20.0 \text{ cm}$
<b>Linac</b>	-
Length of linac (per section)	1.974 m
Number of rf cells	6
Frequency	201.25 MHz
Peak electric field, on axis	15 MV/m
Acceleration at $\phi_s = 90$ degrees	13.4 MeV
Optimum synchronous phase $\phi_s$	28.65 degrees
$\Delta\phi_s$ per section	0 to few deg.
Acceleration at optimum $\phi_s$	12.5 MeV
Beryllium-window thickness	125 $\mu\text{m}$
Radial aperture, linac	$r = 19 \text{ cm}$
<b>Beam from buncher</b>	-
Mean momentum	200 MeV/c
$\epsilon_N$ Normalized transverse emittance, initial	16.9 $\pi$ mm-rad
$\sigma_x$ (lab frame), initial	4.5 cm
$\sigma_{px}$ (lab frame), initial	32 MeV/c
Longitudinal bunch spread (full width)	$\pm 50 \text{ cm}$

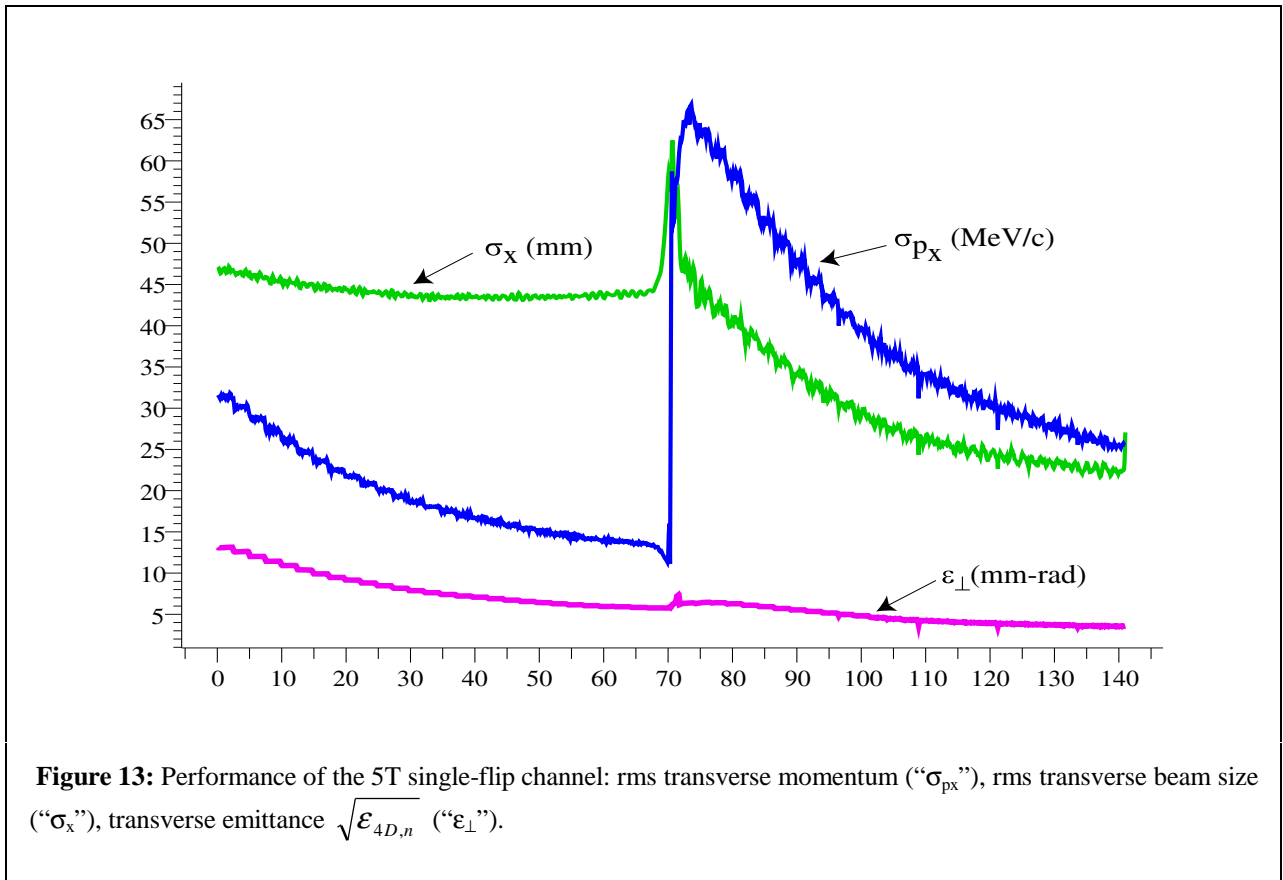
**Table 3:** List of parameters for the 5T single-flip cooler with pillbox cavities. The hydrogen vessel and the linac are centered on the symmetry points of the section, at  $z = 0$  and  $z = \Delta L/2$ , respectively. The parameters of the input beam are listed at the end of the table.

matching section is the most technically challenging component of this cooling channel. The magnetic field at the large-radius coils ( $r = 70$  cm), which run in opposite polarity, is  $\sim 9$  T, while the current density is  $375$  A/mm<sup>2</sup>. The field on the small-radius coils ( $r = 20$  cm) is only 3 T, due to the near-zero average value of the field on axis in this region. The current density for these coils is  $510$  A/mm<sup>2</sup>. While these current densities are reasonable for Nb<sub>3</sub>Sn [14], the hoop stresses on the large-radius coils and the repulsive forces between them are large. This problem will require detailed engineering studies, however, since there is only one field flip in this channel the problem is considered tractable.

### 6.3.3 Performance

The performance of the channel is summarized in Figure 13. This channel cools in 2D by a factor of  $\sim 4$  transversely, from  $16.9\pi$  to  $3.1\pi$  mm-rad, and heats longitudinally by a factor of  $\sim 2$ . As seen in the figure, the first half of the channel reduces the rms transverse momentum of the beam from 32 to 17 MeV/c without changing the size of the beam envelope. The change of field polarity in the matching section causes  $\sigma_{px}$  to grow by a factor of  $\sim 3$ . Due to the displacement of the Larmor orbits, the second supersection cools both  $\sigma_x$  and  $\sigma_{px}$ , to final values of 20 mm and 25 MeV/c, respectively. The second half recovers from the emittance growth in the field-flip region, cools the transverse size of the beam, and restores angular momentum such that the beam is canonical when it exits the cooling section.

Fractional transmission through this channel is approximately 50%. The bunch fills the 201.25-MHz rf bucket from the start, with a full width of  $\pm 1.8$  ns ( $\pm 50$  cm). About half of the lost particles are muons that are not captured into the bucket; these are lost in the first few meters of the cooling channel. The remaining particle loss is due to the excitation of longitudinal motion in the field-flip region, where the longitudinal emittance grows by a factor of 4. Low-momentum muons are lost at the maximum of this synchrotron oscillation,  $\sim 10 - 15$  meters after the matching section. Thus the second part of the channel scrapes longitudinally, resulting in a final full width of  $\pm 2$  ns ( $\pm 60$  cm). At the current stage of optimization the yield within the acceptance of the acceleration (see section 6.1.2) is similar to or slightly better than that in the FOFO case.



## 6.4 Summary

We have studied proposed designs for FOFO and single-flip cooling channels. The FOFO design has been extensively simulated using both DPGeant and ICOOL, and initial simulations of the single-flip channel have been performed using DPGeant. While the two channels have comparable cooling performance within the acceptance of the muon-acceleration system, they achieve that performance in differing ways that will be subject to differing engineering constraints. For example, the single-flip channel offers greater mechanical simplicity, since it has only one field reversal and uses longer absorbers with fewer windows. The two designs also make differing trade-offs between final transverse emittance and longitudinal bucket size: the single-flip channel studied here accelerates the beam during cooling, resulting in a larger bucket and reducing longitudinal losses at the expense of greater losses from the transverse cut imposed by the acceleration system. The implications of these sorts of trade-off are under investigation.

While both designs have adequate performance for an entry-level neutrino factory, both fall short of the PJK benchmark. In both cases, the performance of the cooling channel is limited by the parameters of the input beam provided at the end of the buncher. We expect that ongoing work on tuning and optimization will improve the muon yield by a substantial factor. We note in this regard the very recent work by Palmer *et al.* [15], which suggests that an additional factor 4 or more may be achievable by improvements in the phase rotation and buncher.

## 6.5 Future Steps

### 6.5.1 Cooling theory, simulation, and optimization

Although considerable progress has been made in understanding the problems involved in applying ionization cooling, and designing realistic cooling channels, more work is needed to optimize performance and to minimize cost. In particular, cooling the longitudinal phase space would ease the design requirements for all components of the machine downstream of the cooling section, thus helping to reduce the cost and to design more efficient components. We plan to continue simulation studies and optimizations of existing emittance-exchange concepts [1]. We would also like to consider other configurations, for example, one based on the helicoidal-channel proposal [16]. We plan to continue our work towards eliminating model uncertainties present in our current simulations of the ionization-cooling process. These include the correlations between straggling and large-angle-scattering, the atomic form factors that enter into the calculation of multiple scattering, and the effect of intense magnetic fields on these processes.

In this report we have presented two ionization cooling schemes based on differing design principles. The objective of our study is to design an efficient transverse cooling channel with components that can be built at the present time, or could be developed with a well-defined R&D plan. Detailed simulation studies are required to obtain the optimal solution for each of the available cooling channels. These studies will be crucial in selecting the best design, based on performance, engineering constraints, and cost. In particular, the engineering details of the design of the rf-cavity grids or windows (see Section 6.2.2), and their corresponding electric fields, will be implemented in our simulations. This project will require the use of full 3-dimensional codes and diagnostics to estimate reliably both the effects of scattering off these complicated shapes and the effects of the field on the longitudinal phase space. Evaluating the effect of alignment errors also requires 3D codes. Another project which requires this code development is the study of cooling channels that can achieve longitudinal cooling, because they involve elliptical or wedge-shaped absorbers. In addition, the optimization of each design must respect the engineering constraints on coil current densities, coil placement, and forces on the coils. Successive iterations of our simulation studies with the engineering analysis of each of the design variants will achieve the best solution. The performance of any cooling channel is tightly coupled to the performance of the machine components upstream of it and to the acceptance of the acceleration section that follows. For this reason, the optimization of the cooling channel will have to be iterated with the evolution of the designs of these other components.

### 6.5.2 Magnetic focusing system

The cooling channels described above require high magnetic field strength to reach low  $\beta_{\perp}$  and precise field shape to control the beam dynamics. While we do not plan to rely on new superconducting materials or techniques, the optimization of the magnets demands proper engineering. For instance, a critical limit is the hoop stress on the windings for coils running with opposite currents. We therefore plan to tightly control future designs by obeying these design rules. Improving our knowledge and technical expertise in this area is critical.

### 6.5.3 Absorbers

The baseline (FOFO) cooling design requires liquid-hydrogen absorbers that are thin (~13 cm) relative to their diameter (20 - 30 cm). For a given pressure differential, hemispherical windows are thinnest, however, with this oblate shape thicker ellipsoidal or torispherical windows are required to provide a sufficiently short sagitta (see Section 6.2.2). For such absorbers scattering in the windows is of key importance, requiring R&D on exotic window materials (beryllium and/or AlBeMet) whose safety for LH<sub>2</sub> containment has yet to be established. While the lore within high-energy physics is that beryllium and LH<sub>2</sub> are incompatible, a less absolute view prevails in industry. A program of design studies backed up by carefully-designed tests will be needed to establish safe design and operating parameters for beryllium-containing windows for LH<sub>2</sub> containment. With 40% greater strength than aluminum and 2.1 times the radiation length, AlBeMet has the potential to lower the total radiation-length fraction per absorber from ~2.4% to 1.8% or less, depending on the detailed optimization of absorber dimensions. (While beryllium windows may also be feasible, there appears to be little additional gain in going beyond AlBeMet.)

Other cooling scenarios use absorbers that are thicker compared to their diameter. Here effects of windows on cooling performance are reduced, and aluminum windows may be adequate. Whether R&D on exotic window materials is worthwhile may thus depend on which cooling approach prevails.

In all scenarios the specific power dissipation in the absorbers is large and represents a substantial portion of the cryogenic load of the cooling channel. Handling this heat load is a significant design challenge. An R&D program is already in place at IIT to understand the thermal and fluid-flow aspects of maintaining a constant temperature within the absorber volume despite the large spatial and temporal variations in power density. This program is beginning with computational-fluid-dynamics studies and is planned to proceed to bench tests and high-power beam tests of absorber prototypes over the next year.

In some scenarios (especially those with emittance exchange), lithium hydride (LiH) absorbers may be called for. Since it is a solid, LiH in principle can be fabricated in arbitrary shapes. In emittance-exchange channels, dispersion in the lattice spatially separates muons according to their energies, whereupon specially shaped absorbers can be used to absorb more energy from muons of higher energy and less from those of low energy. However, solid LiH shapes are not commercially available, and procedures for their fabrication would need to be developed. Such an effort is challenging since LiH reacts with water, releasing hydrogen gas and creating an explosion hazard.

### 6.5.4 Beam Diagnostics

Techniques for optimizing the operation of a physical cooling channel must also be developed. Alignment errors in constructing the magnetic system need to be tracked. The beam emittances and particle losses in these cooling channels must be measured in order to optimize running conditions. These beam measurements will be complicated by the large size of the beam, the poor access (see

Figure 4 and Figure 10), high magnetic fields, need for low-temperature insulation, and short bunch structure. This subject has not received attention comparable to other parts of the study, although a preliminary examination of some of these issues has been done [17].

Although measurements of muon beams have been done for years, the high precision, high intensities, limited access, and large backgrounds associated with the cooling channel may make the required measurements difficult. There are a number of measurements that seem to be required in order to optimize the performance of the cooling system. These requirements include: 1) initial matching of the cooling optics to the beam parameters, 2) maintaining this match down the length of the cooling channel, 3) producing and maintaining the physical alignment of beam components, 4) identifying and minimizing transverse and longitudinal loss mechanisms, and 5) measurement of the emittance at various stages of cooling. Since the emittance will only change by a few percent in each cooling section, it may be desirable to have a few special diagnostic sections interspersed with cooling sections to make precise measurements.

One would ideally like high-precision measurements of the six-dimensional muon phase space at a variety of locations along the cooling channel and acceleration system, although the only experimentally available quantities are the transverse and longitudinal bunch profiles. Measurement of the muon emittance from a beam profile is complicated by possible mismatches in the cooling optics which could produce uncertainties in the beta function and the calculated emittance. Measurements could also be complicated by pion and other backgrounds, particularly at the upstream end of the cooling channel.

While many conventional accelerator diagnostics may be appropriate for some applications, it seems desirable to look carefully at secondary emission monitors (SEM's) and Faraday cups. The intense muon beams expected would produce large signals without amplification, and the short range of low-energy muons would permit the option of stopping the beam in a transmission line and looking at the electrical pulse directly. Using one possibly appropriate

geometry, Beck and Schutt [18] have demonstrated an 18-ps rise time with good dynamic range. A variety of options may be available for destructive and non-destructive diagnostics using these principles.

## REFERENCES

- [1] C. M. Ankenbrandt *et al.*, “Status of Muon Collider Research and Development and Future Plans,” *Phys. Rev. ST Accel. Beams*, **2**, 081001, (1999).
- [2] G.I.Budker and A.N.Skrinsky, “Electron cooling and new possibilities in elementary particle physics,” *Sov. Phys. Usp.* **21**, 277 (1978).
- [3] D.Neuffer, *Particle Accelerators* **14**, 75 (1983).
- [4] G. Penn, “Beam Envelope equations in a Solenoidal Field,” MUCOOL Note 71 (<http://www-mucool.fnal.gov/mcnotes/muc0071.ps>).
- [5] R. B. Palmer, C. Johnson and E. Keil, “A cost effective design for a neutrino factory,” **BNL-66971, CERN SL/99-070**, also available at <http://www-mucool.fnal.gov/mcnotes/muc0067.ps>.
- [6] K. J. Kim and C. X. Wang, “Formulae for Transverse Ionization Cooling in Solenoidal Focusing Channels,” MUCOOL Note 92 (<http://www-mucool.fnal.gov/mcnotes/muc0092.ps>).
- [7] R. Fernow, “ICOOL, A simulation Code for Ionization Cooling of Muon Beams,” **Proceedings of the 1999 Particle Accelerator Conference**, A. Luccio, and W. MacKay, eds. (IEEE, Piscataway, NJ, 1999), p. 3020.
- [8] DPGeant is based on the Geant3 simulation tool kit, see <http://www-pat/simulations/muc>; also the “Geant3 User Manual,” <http://wwwinfo.cern.ch/asd/geant/index.html>.
- [9] J. Miller (National High Magnetic Field Laboratory, Florida State University), private communication.
- [10] “ASME Boiler and Pressure Vessel Code,” ANSI/ASME BPV-VIII-1 (American Society of Mechanical Engineers, New York, 1980), part UG-32.
- [11] “Guidelines for the Design, Fabrication, Testing, Installation and Operation of Liquid Hydrogen Targets,” Fermilab, Rev. May 20, 1997; J. Kilmer, private communication.
- [12] J. W. Mark, SLAC-PUB-3169 (1984) and references therein.
- [13] E. J. Beise *et al.*, *Nucl. Instrum. Meth.* A378, 383 (1996).
- [14] I. Bogdanov *et al.* (IHEP Protvino), private communication. Hoop-stress limits [9] may require a design with lower current density.
- [15] See R. B. Palmer *et al.*, <http://pubweb.bnl.gov/people/palmer/nu/pjksim/pjksim.ps>.
- [16] Ya. Derbenev, talk given at the 1999 conference on Muon Collider, San Francisco.
- [17] J. Norem, “Muon Diagnostic issues for the Neutrino Source,” MUCOOL Note 85 (<http://www-mucool.fnal.gov/mcnotes/muc0085.ps>).
- [18] G. Beck and D. W. Schutt, *Rev. Sci. Instr.* **43** (1972) 341.